Analysis of High-throughput Microscopy Videos: Catching Up with Cell Dynamics

A. Arbelle[1], N. Drayman[2], M. Bray[3], U. Alon[2], A. Carpenter[3], and T. Riklin Raviv[1]

[1] Ben-Gurion University of the Negev
[2] Weizmann Institute of Science
[3] Broad Institute of MIT and Harvard

Abstract. We present a novel framework for high-throughput cell lineage analysis in time-lapse microscopy images. Our algorithm ties together two fundamental aspects of cell lineage construction, namely cell segmentation and tracking, via a Bayesian inference of dynamic models. The proposed contribution exploits the Kalman inference problem by estimating the time-wise cell shape uncertainty in addition to cell trajectory. These inferred cell properties are combined with the observed image measurements within a fast marching (FM) algorithm, to achieve posterior probabilities for cell segmentation and association. Highly accurate results on two different cell-tracking datasets are presented.

1 Introduction

High-throughput live cell imaging is an excellent and versatile platform for quantitative analysis of biological processes, such as cell lineage reconstruction. However, lineage analysis poses a difficult problem, as it requires spatiotemporal tracing of multiple cells in a dynamic environment. Since addressing this challenge manually is not feasible for large data sets, numerous cell tracking algorithms have been developed. Forming complete cell tracks based on frame-to-frame cell association is commonly approached by finding correspondences between cell features in consecutive frames. Typical cell properties used for this purpose are cell pose, location and appearance e.g. center of mass (COM), intensity, and shape. As a result, cell segmentation is therefore inevitable, and is thus typically an integral part of the tracking process.

Cell association becomes complicated when the feature similarity of a cell and its within-frame neighbors is comparable to the similarity of the same cell in consecutive frames. When cells cannot be easily distinguished, a more elaborate cell matching criterion is needed, for example, considering cell dynamics [21], solving sub-optimal frame-to-frame assignment problems, via linear programming optimization[8] or by using multiple hypothesis testing (MHT) [17] and its relaxations [7]. In these cases, a two-step approach in which cell segmentation and cell association are treated as independent processes is feasible, provided that the segmentation problem is well-posed and addressed [10,11,12,16,20].

N. Navab et al. (Eds.): MICCAI 2015, Part III, LNCS 9351, pp. 218–225, 2015.
DOI: 10.1007/978-3-319-24574-4_26

Nevertheless, the accurate delineation of cell boundaries is often a challenging task. A high degree of fidelity is required for cell segmentation, even in instances where the cells are far apart and hence can be easily distinguished, especially in cases where the extracted features (e.g. shape or intensity profile) are also the intended subject of the biological experiment. Therefore, several recent methods attempt to support segmentation through solving the cell association problem. For example, the initial cell boundaries in the active contour (AC) framework can be derived from the contours of the associated cells in the previous frame [4]. An alternative AC strategy is to segment a series of time-lapse images as a 3D volume [13]. More recent methods successfully deal with complex data sets using probabilistic frameworks. In the graphical model suggested by [19] cell segments are merged by solving MHT subject to inter-frame and intra-frame constraints. The Gaussian mixture model of [1] is based on the propagation of cell centroids and their approximated Gaussian shape to the following frame in order to combine super-voxels into complete cell regions.

In this paper, cell tracking and segmentation are jointly solved via two intertwined estimators, the Kalman filter and maximum a posteriori probability (MAP). The key idea is a dynamic shape modeling (DSM) by extending the commonly-used Kalman state vector to account for shape fluctuations. Shape inference requires a probabilistic modeling of cell morphology, which is not mathematically trivial. We address this challenge by applying a sigmoid function to the signed distance function (SDF) of the cell boundaries in which the slope of the sigmoid models the shape uncertainty. Given the estimated cell poses, shape models and velocity maps generated from the observed image measurements, we calculate the posterior probabilities of the image pixels via a fast marching (FM) algorithm. Partitioning the image into individual cells and background is defined by the MAP estimates.

The proposed method is mathematically elegant and robust, with just a few parameters to tune. The algorithm has numerous advantages: Estimating the cell temporal dynamics facilitates accurate frame-to-frame association, particularly in the presence of highly cluttered assays, rapid cell movements or sequences with low frame rates. Therefore, unlike the active contour approach, the usability of the segmentation priors is not limited by large displacements or crossing cell tracks. Moreover, the motion estimation allows for lineage recovery in the case of disappearing and reappearing cells, which would otherwise disrupt accurate tracking. The DSM serves as a prior for the consecutive frame segmentation without imposing any predetermined assumptions, in contrast to [1] which implicitly assumes ellipsoidal structures. Furthermore, introducing the boundary uncertainty estimate to the shape model makes our algorithm robust against temporal, morphological fluctuations. Lastly, we note that mitotic events (i.e., cell division) significantly complicate cell tracking. We address this issue by initiating tracks for the daughter cells, using the probabilistic framework to naturally assign a mother cell to its children.

The rest of the paper is organized as follows. In Section 2, we introduce our novel approach which consists of four main components: (1) Extended state

vector estimation via Kalman filter; (2) probabilistic DSM based on previous frame segmentation and the estimated boundary uncertainty; (3) FM algorithm for the calculation of the posterior probabilities; and (4) MAP estimation. Section 3 presents highly accurate experimental results for two different datasets of over 70 frames each, and we conclude and outline future directions in Section 4.

2 Methods

2.1 Problem Formulation

Let $\mathcal{C} = \left\{C^{(1)}, ..., C^{(K)}\right\}$ denote K cells in a time lapse microscopy sequence, containing $\mathcal{T}$ frames. Let $I_t : \Omega \to \mathbb{R}^+$ be the t-th frame, in that sequence, where Ω defines the 2D image domain of I_t, and $t = 1, ..., \mathcal{T}$. We assume that each I_t is a gray-level image of $\mathcal{K}_t$ cells which form a subset of $\mathcal{C}$. Our objective is twofold and consists of both cell segmentation and frame-to-frame cell association defined as follows:

Segmentation: For every frame I_t, find a function $f_t \colon \Omega \to L_t$, (where L_t is a subset of $\mathcal{K}_t + 1$ integers in $[0, \ldots, K]$) that assigns a label $l_t \in L_t$ to each pixel $\mathbf{x} = [x, y] \in \Omega$. The function f_t partitions the t-th frame into $\mathcal{K}_t + 1$ regions, where each segment $\Gamma_t^{(k)} = \{\mathbf{x} \in \Omega | f_t(\mathbf{x}) = l_t = k, \}$ forms a connected component of pixels, in frame I_t, that belongs to either a specific cell in $\mathcal{C}$ or to the background, i.e. $\Gamma_t^{(0)}$.

Association: For every frame I_t find an injective function $h_t : L_{t-1} \to L_t$ that corresponds cell segments in frame $t-1$ and frame t. As we will show in the following, the segmentation and association steps are merged and $\Gamma_t^{(k)}, k \geq 1$ defines the segmentation of cell $C^{(k)}$ in frame t.

2.2 Time Series Analysis

For every cell $C^{(k)}$ there exist a number of properties that describe its state at a given time t. Let $\xi_t^{(k)}$ denote the hidden state vector that holds the true, unknown, state of the cell. In the following discussion the superscript (k) is removed for clarity. In our case the state vector holds the following features:

$$\xi_t = [c_{x_t}, c_{y_t}, v_{x_t}, v_{y_t}, \epsilon_t]^T = \left[\mathbf{c}_t^T, \mathbf{v}_t^T, \epsilon_t\right]^T \tag{1}$$

where $\mathbf{c}_t = [c_{x_t}, c_{y_t}]^T$ denote the COM of the cell at time t and $\mathbf{v}_t = [v_{x_t}, v_{y_t}]^T$ denote the COM velocities. The variable ϵ_t is the shape uncertainty variable, which will be explained in section 2.3. We assume that the state vector approximately follows a linear time step evolution as follows: $\xi_t = \mathrm{A}\xi_{t-1} + w_{t-1}$, where $\mathrm{A} \in \mathbb{R}^{5\times5}$ is the state transition model, and $w_t \in \mathbb{R}^5$ is the process noise drawn i.i.d from $\mathcal{N}(\mathbf{0}, \mathrm{Q}_t)$. In our case: $A_{i,i} = 1, i = 1 \ldots 5$; $A_{1,3} = A_{2,4} = 1$. Since the true state is hidden, the observed state is $\zeta_t = \xi_t + r_t$, where $r_t \in \mathbb{R}^5$ is the measurement noise drawn i.i.d from $\mathcal{N}(\mathbf{0}, \mathrm{R}_t)$. The process and measurement noise covariance matrices $\mathrm{Q}_t, \mathrm{R}_t$ are assumed to be known.

In order to predict the state of a cell at t we utilize the Kalman Filter [9]. The predicted (a priori) state vector estimation and error covariance matrix at t given measurements up to time $t-1$ are: $\hat{\xi}_{t|t-1} = \mathrm{A}\hat{\xi}_{t-1|t-1}$; $\Sigma_{t|t-1} = \mathrm{A}\Sigma_{t-1|t-1}\mathrm{A}^T + \mathrm{Q}_t^T$

The a posteriori state estimate and error covariance matrix at time t given measurements up to and including time t are: $\hat{\xi}_{t|t} = \hat{\xi}_{t|t-1} + G_t\left(\zeta_t - \hat{\xi}_{t|t-1}\right)$; $\Sigma_{t|t} = (\mathrm{I} - G_t\mathrm{B})\,\Sigma_{t|t-1}$

where the Kalman Gain matrix is given as: $\mathrm{G}_t = \Sigma_{t|t-1}\left(\Sigma_{t|t-1} + \mathrm{R}_t\right)^{-1}$.

2.3 Dynamic Shape Model

The estimated segmentation of a cell $C^{(k)}$ in frame t, i.e. $\hat{\Gamma}_{t|t-1}^{(k)}$ is obtained by a translation of the cell segmentation in frame $t-1$:

$\hat{\Gamma}_{t|t-1}^{(k)} = \left\{\mathbf{x}|\left(\mathbf{x} - \hat{\mathbf{v}}_{t|t-1}^{(k)}\right) \in \Gamma_{t-1}^{(k)}\right\}$, where, $\hat{\mathbf{v}}_{t|t-1}^{(k)} \cdot 1$, is the estimated cell displacement. The respective signed distance function (SDF) $\hat{\phi}_{t|t-1}^{(k)} : \Omega \to \mathbb{R}$ is constructed as follows:

$$\hat{\phi}_{t|t-1}^{(k)}(\mathbf{x}) = \begin{cases} \min_{\mathbf{x}' \in \partial\hat{\Gamma}_{t|t-1}^{(k)}} d_E(\mathbf{x}, \mathbf{x}') & \mathbf{x} \in \hat{\Gamma}_{t|t-1}^{(k)} \\ -\min_{\mathbf{x}' \in \partial\hat{\Gamma}_{t|t-1}^{(k)}} d_E(\mathbf{x}, \mathbf{x}') & \mathbf{x} \notin \hat{\Gamma}_{t|t-1}^{(k)} \end{cases} \tag{2}$$

where $d_E(\cdot,\cdot)$ denotes the Euclidian distance and $\partial\hat{\Gamma}_{t|t-1}$ denotes the estimated segmentation boundary. In the spirit of [18,15], we define the probability that a pixel $\mathbf{x}$ belongs to the domain of cell k by a logistic regression function (LRF):

$$\hat{\Phi}_{t|t-1}^{(k)}(\mathbf{x}) = P\left(\mathbf{x} \in \Gamma_t^{(k)}\right) \triangleq \left(1 + \exp\left\{-\frac{\hat{\phi}_{t|t-1}^{(k)}(\mathbf{x})}{\hat{\epsilon}_{t|t-1}^{(k)}}\right\}\right)^{-1} \tag{3}$$

where, $\hat{\epsilon}_{t|t-1}^{(k)}$ is the estimation of $\epsilon_t^{(k)} \triangleq d_H\left(\partial\Gamma_{t-1}^{(k)}, \partial\Gamma_t^{(k)}\right) \cdot \frac{\sqrt{3}\pi}{2}$ which denotes the calculated[1] boundary uncertainty. The LRF slope is determined by $\epsilon_t^{(k)}$. We set $\epsilon_t^{(k)}$ such that the standard deviation of the probability density function (PDF) corresponding to $P\left(\mathbf{x} \in \Gamma_t^{(k)}\right)$ is equal to the Hausdorff distance between the aligned cell boundaries i.e. $d_H\left(\partial\Gamma_{t-1}^{(k)}, \partial\Gamma_t^{(k)}\right)$. Note, that large temporal fluctuations in a cell boundary, increase d_H, which in turn smooth the LRF slope and increase the shape uncertainty. Eq.3 defines our dynamic shape model.

2.4 MAP Segmentation and Association

We now present the flow of the proposed segmentation algorithm given the state vector estimation $\hat{\xi}_{t|t-1}$ and cell segmentation of the previous frame. Fig.1 illustrates the main concepts to be discussed. Consider the image I_t with $\mathbf{c}_t^{(k)}$ marked

[1] Derived from an analytic expression. See appendix A.1.

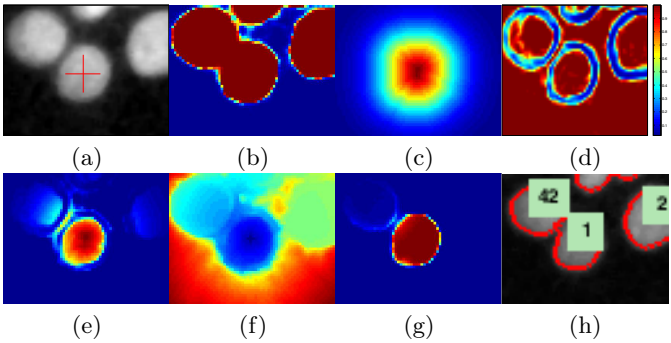

Fig. 1. Segmentation flow of a specific cell. (a) Original image. The estimated COM of the specific cell k is marked by red cross. (b) Intensity probability of the foreground P_{FG}. (c) DSM (Spatial probability). (d) Traversability image $g\left(\nabla_{\mathbf{x}} I_t\right)$. (e) Speed image $\hat{S}^{(k)}_{t|t-1}$, the product of (b-d). (f) FM distance. (g) DSM posterior $P^{(k)}_t$ (h) Labeled segmentation.

by a red cross, shown in Fig.1.a. We model the PDFs of the foreground and background intensities, $f_{FG}\left(\cdot\right)$ and $f_{BG}\left(\cdot\right)$ respectively by a mixture of Gaussians. The intensity based probability of being a cell or background (Fig.1.b) is defined as follows:

$$P^{(BG)}_t\left(\mathbf{x}\right) = \frac{\alpha f_{BG}\left(I_t\left(\mathbf{x}\right)\right)}{\alpha f_{BG}\left(I_t\left(\mathbf{x}\right)\right) + \left(1-\alpha\right) f_{FG}\left(I_t\left(\mathbf{x}\right)\right)}; \; P^{(FG)}_t\left(\mathbf{x}\right) = 1 - P^{(BG)}_t\left(\mathbf{x}\right) \tag{4}$$

where $0 < \alpha < 1$ is a predetermined weight (we set $\alpha = 0.5$).

For each cell segment, in frame t, we construct a DSM, $\hat{\Phi}^{(k)}_{t|t-1}$, as explained in section 2.3 (Fig.1.c). We use the FM algorithm [6] to find the shortest path from each pixel $\mathbf{x}$ to the estimated COM of a cell k s.t. a speed image $\hat{S}^{(k)}_{t|t-1} : \Omega \rightarrow [0,1]$ (Fig.1.e). The FM distance, $d_{FM}\left(\mathbf{x}, \hat{\mathbf{c}}^{(\mathbf{k})}_{t|t-1} | \hat{S}^{(k)}_{t|t-1}\right)$, is the minimal geodesic distance from $\mathbf{x}$ to $\hat{\mathbf{c}}^{(\mathbf{k})}_{t|t-1}$ (Fig.1.f). In other words, the value of $\hat{S}^{(k)}_{t|t-1}(\mathbf{x})$ is the speed of a pixel $\mathbf{x}$ along the shortest path to $\hat{\mathbf{c}}^{(\mathbf{k})}_{t|t-1}$. For each pixel $\mathbf{x}$ in frame t we define its speed $\hat{S}^{(k)}_{t|t-1}(\mathbf{x})$ as the product of three terms: 1. The intensity based probability of belonging to the foreground (Eq.4). 2. The spatial prior of being part of a specific cell i.e. the DSM (Eq.3). 3. The "traversability" (Fig.1.d) which is inverse proportional to the image edges in frame I_t and defined by $g\left(\nabla_{\mathbf{x}} I_t\right) = \left(1 + \frac{\left|\nabla_{\mathbf{x}} I_t\right|}{\left\|\nabla_{\mathbf{x}} I_t\right\|_2}\right)^{-2}$:

$$\hat{S}^{(k)}_{t|t-1} = P^{(FG)}_t \cdot \hat{\Phi}^{(k)}_{t|t-1} \cdot g\left(\nabla_{\mathbf{x}} I_t\right) \tag{5}$$

The absolute value of the spatial gradient, i.e. $\left|\nabla_{\mathbf{x}} I_t\right|$, can be interpreted as "speed bumps" which make the "FM journey" more difficult across edges.

The posterior probability that $\mathbf{x}$ belongs to C_k is inverse proportional[2] to the difference between its geodesic and Euclidean distances to $\hat{\mathbf{c}}_{t|t-1}^{(\mathbf{k})}$ (Fig.

$$P_t^{(k)}(\mathbf{x}) \propto \left(d_{FM}\left(\mathbf{x}, \hat{\mathbf{c}}_{t|t-1}^{(k)} | \hat{S}_{t|t-1}^{(k)},\right) - d_E\left(\mathbf{x}, \hat{\mathbf{c}}_{t|t-1}^{(k)}\right) + 1\right)^{-1} \tag{6}$$

The final segmentation is given as the MAP of (6)(Fig.1.h): $\Gamma_t^{(k)} = \left\{\mathbf{x} | \arg\max_{k' \in L_t} P_t^{(k')}(\mathbf{x}) = k\right\}$. In fact, we see that cell association is inherent to the defined segmentation problem, since each cell is segmented using its estimated properties from the previous frame. The detection of new cells is explained in appendix A.3.

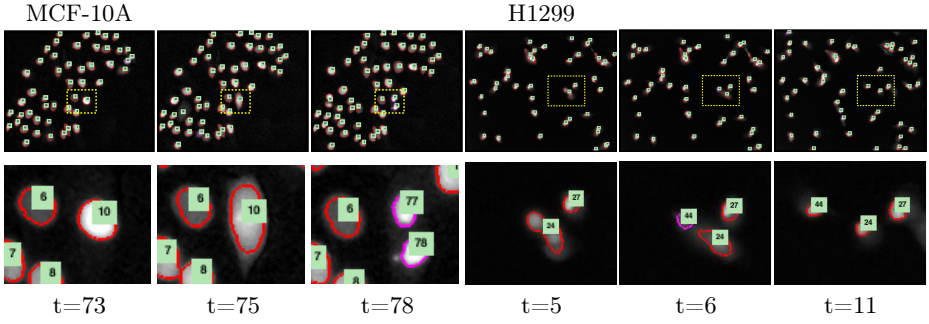

Fig. 2. Top row: A full-frame temporal sequence. Bottom row: Enlargement of inset shown in the top row. Note that mitosis of cells 10 and 24.

3 Experimental Results

We examined two different sequences: (1) MCF-10A cells, expressing RFP- Geminin and NLS- mCerulean, rate: 3fph, 142 frames. (2) H1299 cells, expressing eYFP-DDX5 in the background of an mCherry tagged nuclear protein, rate: 3fph, 72 frames [3]. The input to the algorithm is a manual segmentation of the first two frames of each sequence. We tested our method based on manual annotation generated by an expert. We then compared precision, recall and F-measure scores to those obtained by the maximum correlation thresholding segmentation [14] and linear-assignment problem tracking [7] method as implemented in CellProfiler [2] which is a publicly-available, state of the art, cell analysis tool.

Figure 2 present two sets of sampled frames from the examined data sets. The cell numbers along with the segmentation boundaries are marked. We use purple and red for new and existing tracks, respectively. The upper rows show the full frames, the marked rectangle is magnified in the lower rows. The detected cell trajectories of both data sets can be visualized in Fig.1 in the supplementary material. We note that the noisy linear motion of the cells supports the use of

[2] $P_t^{(k)}(\mathbf{x})$ is normalized such that $\sum_{k'} P_t^{(k')}(\mathbf{x}) = 1$. See appendix A.2.

Table 1. Segmentation and Tracking Results.C.P. is CellProfiler [2] Prc. is Precision, Rcl. is Recall, F is F-measure. Further details can be found in the supp. material.

Data	Method	Segmentation			Full Tracks	Divisions		
		Prc.	Rcl.	F	Success Rate	Prc.	Rcl.	F
H1299	Ours	**0.98**	**0.89**	**0.93**	**0.95**	0.84	0.89	0.86
	C.P	0.93	0.81	0.87	0.86	0.84	0.94	0.88
MCF-10A	Ours	**1**	**0.94**	**0.97**	**0.99**	**0.96**	**0.98**	**0.97**
	C.P	0.98	0.82	0.89	0.94	0.86	0.94	0.90

the Kalman filter. We urge the reader to refer to our live cell segmentation and tracking videos at http://youtu.be/ORx82dCKWlA and in the supplementary material. We quantitatively evaluate our segmentation and mitosis detection as described in [19]. The tracking success was calculated as percentage of full, error-less tracks which were manually counted by an expert. An error was defined as early termination of a track, a split or a merge of tracks. See Table 1 for results.

4 Summary and Conclusions

We address cell segmentation and tracking by jointly solving MAP and Kalman filtering estimation problems. A key contribution is a DSM which accommodates versatile cell shapes with varying levels of uncertainty. The DSM is inferred via time-series analysis and is exploited as a shape prior in the segmentation process. The proposed model can handle long sequences in an elegant and robust manner, requiring minimal input. While the daughters of divided cells are accurately detected, mitotic events are not yet labeled as such. Future work will aim to complete the missing link for cell lineage reconstruction in the spirit of [5] .

Acknowledgments. This work was supported in part by Human Frontiers in Science Program RGP0053/2010 (Carpenter), and NSF RIG DBI 1119830 (Bray) and the Human Frontiers in Science Program RGP0020/2012 (Alon).

References

1. Amat, F., Lemon, W., Mossing, D.P., McDole, K., Wan, Y., Branson, K., Myers, E.W., Keller, P.J.: Fast, accurate reconstruction of cell lineages from large-scale fluorescence microscopy data. Nature Methods (2014)
2. Carpenter, A.E., Jones, T.R., Lamprecht, M.R., Clarke, C., Kang, I.H., Friman, O., Guertin, D.A., Chang, J.H., Lindquist, R.A., Moffat, J., et al.: Cellprofiler: image analysis software for identifying and quantifying cell phenotypes. Genome Biology 7(10), R100 (2006)
3. Cohen, A.A., Geva-Zatorsky, N., Eden, E., Frenkel-Morgenstern, M., Issaeva, I., Sigal, A., Milo, R., Cohen-Saidon, C., Liron, Y., Kam, Z., et al.: Dynamic proteomics of individual cancer cells in response to a drug. Science 322(5907), 1511–1516 (2008)
4. Dzyubachyk, O., van Cappellen, W.A., Essers, J., Niessen, W.J., Meijering, E.: Advanced level-set-based cell tracking in time-lapse fluorescence microscopy. IEEE Trans. on Medical Imaging 29(3), 852–867 (2010)

5. Gilad, T., Bray, M., Carpenter, A., Riklin-Raviv, T.: Symmetry-based mitosis detection in time-lapse microscopy. In: IEEE International Symposium on Biomedical Imaging: From Nano to Macro (2015)
6. Hassouna, M.S., Farag, A.A.: Multistencils fast marching methods: A highly accurate solution to the eikonal equation on cartesian domains. IEEE Trans. on Pattern Analysis and Machine Intelligence 29(9), 1563–1574 (2007)
7. Jaqaman, K., Loerke, D., Mettlen, M., Kuwata, H., Grinstein, S., Schmid, S.L., Danuser, G.: Robust single-particle tracking in live-cell time-lapse sequences. Nature Methods 5(8), 695–702 (2008)
8. Kachouie, N.N., Fieguth, P.W.: Extended-hungarian-jpda: Exact single-frame stem cell tracking. IEEE Trans. Biomed. Eng. 54(11), 2011–2019 (2007)
9. Kalman, R.E.: A new approach to linear filtering and prediction problems. J. of Fluids Engineering 82(1), 35–45 (1960)
10. Kanade, T., Yin, Z., Bise, R., Huh, S., Eom, S., Sandbothe, M.F., Chen, M.: Cell image analysis: Algorithms, system and applications. In: 2011 IEEE Workshop on Applications of Computer Vision (WACV), pp. 374–381. IEEE (2011)
11. Maška, M., Ulman, V., Svoboda, D., Matula, P., Matula, P., Ederra, C., Urbiola, A., España, T., Venkatesan, S., Balak, D.M., et al.: A benchmark for comparison of cell tracking algorithms. Bioinformatics 30(11), 1609–1617 (2014)
12. Meijering, E., Dzyubachyk, O., Smal, I., et al.: Methods for cell and particle tracking. Methods Enzymol. 504(9), 183–200 (2012)
13. Padfield, D., Rittscher, J., Roysam, B.: Spatio-temporal cell segmentation and tracking for automated screening. In: IEEE International Symposium on Biomedical Imaging: From Nano to Macro, pp. 376–379. IEEE (2008)
14. Padmanabhan, K., Eddy, W.F., Crowley, J.C.: A novel algorithm for optimal image thresholding of biological data. J. of Neuroscience Methods 193(2), 380–384 (2010)
15. Pohl, K.M., Fisher, J., Shenton, M.E., McCarley, R.W., Grimson, W.E.L., Kikinis, R., Wells, W.M.: Logarithm odds maps for shape representation. In: Larsen, R., Nielsen, M., Sporring, J. (eds.) MICCAI 2006. LNCS, vol. 4191, pp. 955–963. Springer, Heidelberg (2006)
16. Rapoport, D.H., Becker, T., Mamlouk, A.M., Schicktanz, S., Kruse, C.: A novel validation algorithm allows for automated cell tracking and the extraction of biologically meaningful parameters. PloS One 6(11), e27315 (2011)
17. Reid, D.B.: An algorithm for tracking multiple targets. IEEE Transactions on Automatic Control 24(6), 843–854 (1979)
18. Riklin-Raviv, T., Van Leemput, K., Menze, B.H., Wells, W.M., Golland, P.: Segmentation of image ensembles via latent atlases. Medical Image Analysis 14(5), 654–665 (2010)
19. Schiegg, M., Hanslovsky, P., Haubold, C., Koethe, U., Hufnagel, L., Hamprecht, F.A.: Graphical model for joint segmentation and tracking of multiple dividing cells. Bioinformatics, page btu764 (2014)
20. Su, H., Yin, Z., Huh, S., Kanade, T.: Cell segmentation in phase contrast microscopy images via semi-supervised classification over optics-related features. Medical Image Analysis 17(7), 746–765 (2013)
21. Yang, X., Li, H., Zhou, X.: Nuclei segmentation using marker-controlled watershed, tracking using mean-shift, and kalman filter in time-lapse microscopy. IEEE Trans. Circuits Syst. I, Reg. Papers 53(11), 2405–2414 (2006)